

Factors governing interfacial reactions in liquid metal/non-oxide ceramic systems: Ni-based alloy–Ti/sintered AlN system

A. Koltsov, F. Hodaj*, N. Eustathopoulos

SIMAP - UMR CNRS 5266, INP Grenoble-UJF, Domaine Universitaire, BP 75 - 1130, rue de la Piscine, 38402 Saint Martin d'Hères Cedex, France

Received 16 April 2008; received in revised form 6 June 2008; accepted 11 June 2008

Available online 23 July 2008

Abstract

Wetting of ceramics by liquid metals is often promoted using alloying elements which form at the interface, by reaction with the ceramic, continuous layers of a better wetted compound. These layers can, in turn, improve or be detrimental to the mechanical performance of the interface, depending on their microstructure and thickness.

The aim of this investigation is to determine the factors governing the growth kinetics in metal/non-oxide ceramic systems in which strong reactivity is often observed. The study system consists of a predominantly covalent ceramic, AlN, and a Ni-based liquid alloy containing Ti. Experiments are performed by varying the temperature, Ti content of the alloy and level of vacuum in the furnace. Point experiments were also carried out for a Au based alloy–Ti/AlN and AgZr/AlN couples.

© 2008 Elsevier Ltd. All rights reserved.

Keywords: Wetting; Interface; Diffusion; Joining; Nitrides

1. Introduction

Iono-covalent ceramics such as oxides, carbides or nitrides are generally poorly wetted by liquid engineering metals such as nickel, copper or tin: contact angles are typically higher (and often much higher) than 90° .¹ The complications that produces in material processes such as infiltration or brazing have motivated the search for ways of lowering the contact angle in such systems.

One approach to this end is to alloy the metal with elements that, by reacting with the ceramic, form a better wetted compound at the interface. On alumina substrates for example, the titanium alloyed in a molten copper–silver eutectic reacts with the alumina to form the metallic $\text{Cu}_3\text{Ti}_3\text{O}$ compound that is well wetted by the alloy.²

As has been argued previously (see for instance the recent review in Ref.³), the spreading kinetics in such systems is controlled by the rate at which the reaction product layer can grow parallel to the interface at a region of submicronic size around the solid/liquid/vapour triple line (TL). As the liquid has a direct

access to a fresh solid surface at this line, the reaction rate parallel to the interface is much higher than the reaction rate at the interface behind TL where the reaction product thickening occurs by diffusion through the layer. Note that while the interfacial reaction behind the triple line does not affect (or affects only weakly) wetting and spreading, it can affect other properties of the metal/ceramic couple, namely the thermal resistance of the junction or again the mechanical behaviour of the system. For instance several experimental results, reviewed in Ref.⁴ indicate that exacerbating the thickening of the reaction layer can be detrimental to the mechanical properties of the system.

This study is focused on the reactivity at interfaces behind the triple line formed by liquid metals and non-oxide, predominantly covalent ceramics. A common feature of these ceramics is the high reactivity observed in many cases with alloys containing Ti, Cr or V. For example, at temperatures close to 1100°C , reaction layers several tens of microns thick were observed to form in a few minutes or tens of minutes at interfaces between these alloys and SiC,^{5,6} Si_3N_4 ,^{7–9} AlN^{9,10} or BN.^{9,11} Of particular interest are the results obtained at the same temperature with SiC for two Cr containing alloys, one solid¹² the other liquid.⁵ In this case, while the thermodynamic driving force for the reaction is higher for the solid alloy, the reaction rate for this alloy is one order of magnitude lower than for the liquid alloy.

* Corresponding author.

E-mail address: fhodaj@ltpcm.inpg.fr (F. Hodaj).

This example underlines the role of kinetic factors in interfacial reactivity.

The ceramic studied in the present investigation is sintered AlN. The liquid phase consists of a Ni-based matrix containing a few per cent of Ti. The results concerning wetting and spreading kinetics of these alloys on AlN, obtained by the sessile drop technique, were presented previously.¹³ It was found that, by reaction with AlN, Ti forms a continuous layer of TiN, a nitride of partly metallic character relatively well wetted by the metal. The spreading rate in this system is limited by the AlN dissolution in the molten alloy in the immediate vicinity of the triple line and it is strongly affected by oxygen pollution of the very first surface layers (few nanometres) of the ceramic.¹³ This paper presents results on the growth kinetics of the TiN layer at the interface behind the triple line and on the influence of temperature, Ti content of the alloy and level of vacuum in the furnace on this kinetics. Point experiments were also carried out for AuNiTi/AlN and AgZr/AlN couples. The results are used in order to determine the factors that govern reaction kinetics in this type of interface.

2. Experimental procedure

Experiments were performed by the sessile drop technique in two different furnaces: (i) a metallic furnace, under a vacuum of 10^{-5} Pa, consisting essentially of a molybdenum heater surrounded by molybdenum radiation shields, located in a water-cooled stainless steel chamber, and (ii) an alumina chamber furnace, under a vacuum of 10^{-4} Pa, heated externally by a silicon carbide resistor.

AlN samples were produced by isostatic compression (Ceramiques & Composites, France) starting from AlN powder containing 1 wt% of oxygen with 3–5 wt% Y_2O_3 as sintering aid. The residual porosity is less than 2% and the grain size is in the range 4–10 μm . AlN substrates contain about 1 wt% oxygen either in the AlN lattice or at grain boundaries.¹⁴ AlN samples 0.7 mm thick were mechanically polished using diamond paste up to an average roughness R_a of about 30 nm measured over an area of $250 \mu\text{m} \times 200 \mu\text{m}$. From the XPS and SIMS analysis of AlN surfaces given previously,¹⁵ it was concluded that, after polishing, they are made up of oxide secondary phases at grain boundaries and AlN grains covered by a pollution layer of AlO_xN_y a few tens of nm thick.

The main reactive alloy used in this study is a Ni-based alloy containing 12 at% Si and 4.5 at% Ti named hereafter M–12Si–4.5Ti, the composition of the master alloy M is Ni–3.1Fe–7.8Cr (at%). The M–12Si–4.5Ti alloy was prepared by inductive melting of pure elements Ni (99.99%), Fe (99.99%), Cr (99.97%), Si (99.999%) and Ti (99.7%) under pure Argon in a cold crucible.

Standard sessile drop experiments consist in placing a piece of M–12Si–4.5Ti alloy on an AlN substrate and monitoring by a CDD camera the time-dependent variation in contact angle θ and drop base radius R during continuous temperature rise and isothermal holding in high vacuum.¹³ Some experiments were also performed with a M–12Si–10Ti (at%) alloy prepared in situ by melting a piece of a M–Si alloy with a piece of Ti

over M–Si on the AlN substrate. The M–Si alloy was prepared by processing first the master alloy M from pure elements Ni, Fe and Cr by melting in an alumina crucible at 1500 °C under H_2 and, then melting M and pure Si on an alumina substrate at 1320 °C under secondary vacuum.

Experiments were performed at $T=1250$ °C with alloy masses varying from 40 mg to 90 mg. Two specific experiments were performed at 1215 °C and 1300 °C, respectively.

For comparison purposes, a limited number of experiments were also performed with reactive alloys Ag–1 at% Zr and Au–Ni–5 at% Ti on AlN. The Ag–1 at% Zr was prepared in situ by melting a piece of pure Ag with a piece of Ag–3 at% alloy over Ag on the AlN substrate. The Ag–3 at% alloy was prepared by melt-spinning high purity silver (99.999 wt%) and zirconium (99.99 wt%). The Au–Ni–5 at% Ti alloy was prepared in situ by melting a piece of Au–42.5 at% Ni alloy with a piece of Ti over Au–Ni alloy on the AlN substrate. The Au–42.5 at% Ni alloy, corresponding to the azeotropic composition in the phase diagram, was prepared prior to the experiments by melting pieces of Au–Ni alloy on pure alumina substrates in high vacuum.

After the experiments, specimens were sectioned, embedded in resin and polished for optical and SEM observation on the cross-section and microprobe analysis.

3. Results

3.1. Description of a typical experiment

Fig. 1 gives the variation in contact angle θ and drop base radius R versus time for an experiment carried out at 1250 °C with a M–12Si–4.5Ti (at%) alloy on AlN. It can be seen that R increases from $R=R_0$ corresponding to the complete melting of the alloy to $R=R_F$ at the end of the experiment. For points lying

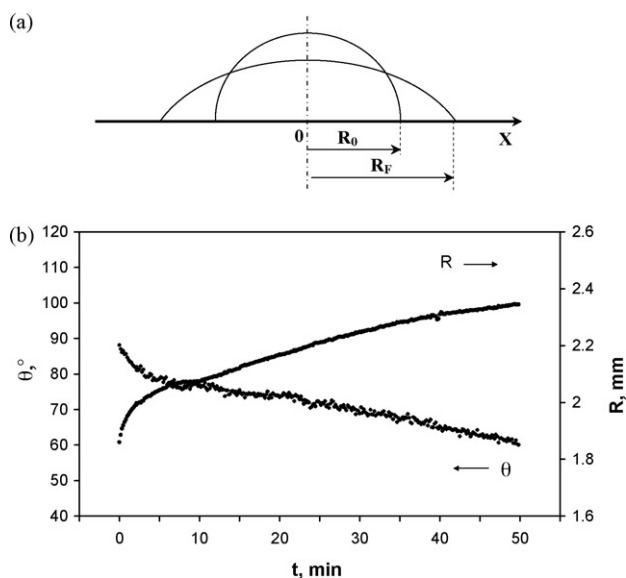


Fig. 1. (a) Schematic droplet profiles: at complete melting ($R=R_0$) and at the end of experiment ($R=R_F$). (b) Contact angle θ and drop base radius R as a function of time for a M–12Si–4.5Ti (at%) alloy on AlN at 1250 °C, metallic furnace. $t=0$ is taken to be complete melting.

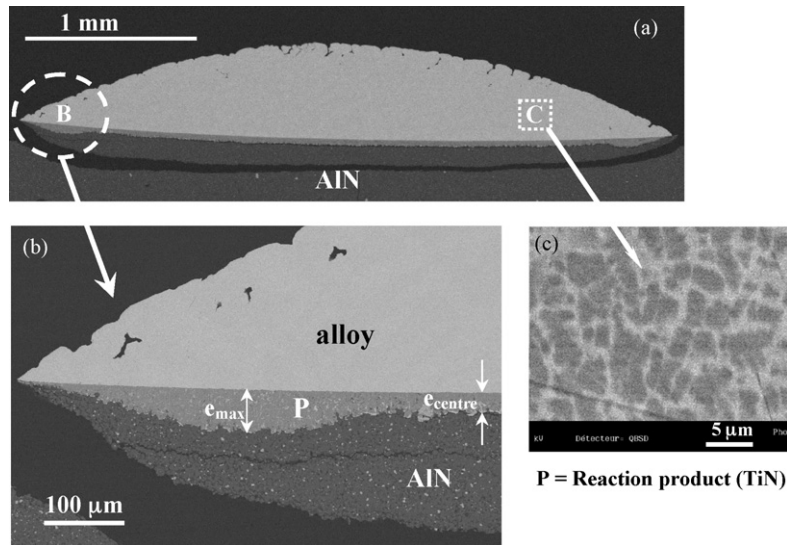


Fig. 2. (a) SEM micrograph of a cross-section of a M-12Si-4.5Ti (at%) alloy on AlN substrate. The crack path is inside AlN. (b) Enlargement of zone B in the micrograph (a). (c) Enlargement of zone C in the micrograph (a). $T = 1250\text{ }^{\circ}\text{C}$, $t = 300\text{ min}$, metallic furnace (backscattered electron image). P denotes the reaction product (TiN). The thicknesses e_{centre} and e_{max} are also indicated in this figure.

at the interface at a distance X from the centre of the drop, the reaction time is equal to the holding time for $-R_0 \leq X \leq +R_0$ and it decreases from holding time at $R = R_0$ to zero at $R = R_F$. In the following, reactivity at the interface centre is taken to mean reactivity at $-R_0 \leq X \leq +R_0$. The other wetting experiments are given in Ref.¹³

3.2. Metallic furnace ($P = 10^{-5}\text{ Pa}$)

All experiments in this furnace were carried out with the M-12Si-4.5Ti alloy. The influence of reaction time and temperature on the morphology and growth kinetics of the reaction product was studied for contact times up to 300 min and temperatures varying from $1215\text{ }^{\circ}\text{C}$ to $1300\text{ }^{\circ}\text{C}$.

3.2.1. Morphology, microstructure and interface composition

Fig. 2a and b give SEM micrographs of an M-12Si-4.5Ti/AlN sample after an experiment lasting 300 min at $1250\text{ }^{\circ}\text{C}$ showing that a reaction product layer is formed at the interface. The thickness (e) of this layer is almost uniform over most of the interface around the drop centre ($e_{\text{centre}} \approx 30\text{ }\mu\text{m}$) and has a maximum value in a region close to the triple line ($e_{\text{max}} \approx 45\text{ }\mu\text{m}$). The drop bulk microstructure is made up of a eutectic matrix and grey dendrites (see Fig. 2c) each of which represents about 50% of the total alloy volume. According to the microprobe analysis the grey dendrites contain 0.3 at% Ti and 3.3 at% Al, while the matrix about 0.2 at% Ti and 1.6 at% Al.

Two cross-sections of the interfacial region close to the drop centre are shown in Fig. 3a and b for experiments performed at $1250\text{ }^{\circ}\text{C}$ for 20 and 50 min, respectively. In Fig. 3a, the reaction zone appears to consist of titanium nitride grains separated by metallic films a few hundreds of nm thick. These films are rich in nickel alloy and contain significant amounts of alu-

minium. A careful examination of the reaction product zone close to AlN showed that this zone in fact also consists of titanium nitride grains surrounded by metallic films but with a finer microstructure. Moreover, at the AlN/layer interface, several metallic inclusions a few micrometers in size can be seen. These inclusions cover a large part of this interface. Fig. 3b shows that the inert micrometric Y_2O_3 particles, initially included in the AlN substrate, are observed over the entire reaction layer.

In this system, Ti contained in the alloy can react with the AlN substrate to form titanium nitride according to the reaction: $(\text{Ti}) + (\text{AlN}) \rightarrow (\text{Al}) + (\text{TiN}_{1-x})$. The notations $(\)$ and $(\)$ designate the solid and liquid states, respectively. The subscript

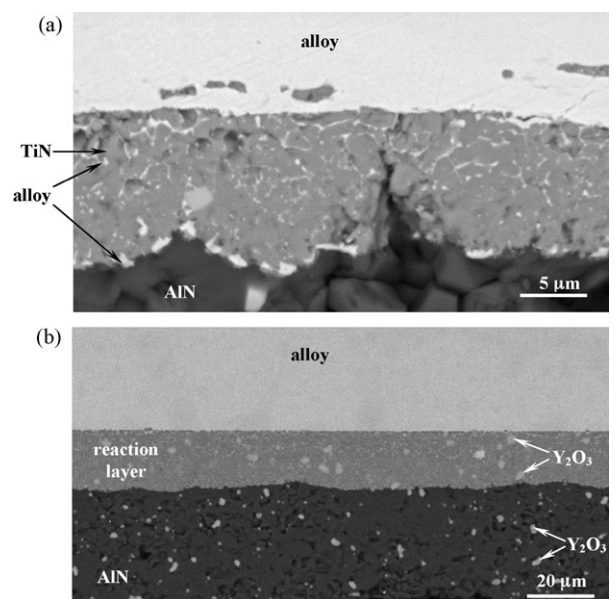


Fig. 3. SEM micrographs of cross-sections of M-12Si-4.5Ti/AlN samples. $T = 1250\text{ }^{\circ}\text{C}$, metallic furnace (a) $t = 20\text{ min}$, (b) $t = 50\text{ min}$ (backscattered electron images).

Table 1
Thickness of the reaction layer formed at the M–12Si–4.5Ti/AlN interface at the centre of the drop (e_{centre}) and maximum of this thickness observed at regions close to the triple line (e_{max}) – see Fig. 2a and b – for different reaction times at 1250 °C

t (min)	0	10	20	35	50	300
e_{centre} (μm)	0.9 ± 0.7	5.3 ± 1.5	11 ± 2	10.9 ± 2.5	16.5 ± 2	29 ± 2
$e_{\text{max}}^{\text{a}}$ (μm)	–	–	Broken sample	22.8 ± 1.6	24 ± 0.4	44 ± 0.7

Experiments performed in a metallic furnace ($P = 10^{-5}$ Pa). $t = 0$ corresponds to an experiment stopped immediately after the temperature attained 1250 °C.

^a Mean value calculated from two maxima formed to the left and right of the interface (see Fig. 2a).

x denotes the deviation from the stoichiometric composition of TiN. The value of x is determined by the thermodynamic activity of Ti in the alloy.¹⁶

It should be noted that, during this reaction, titanium consumption in the drop can be considerable, especially for long-term experiments, thereby leading to aluminium enrichment of the drop. For example, in the sessile drop configuration and for contact angles close to 70° (Fig. 1), a simple mass balance indicates that when a 10 μm thick TiN layer forms at the interface, the expected decrease in Ti content of the drop would be about 1.4 at% Ti or 0.7 at% for a 45 or 90 mg droplet, respectively. This is in agreement with the final Ti content of about 0.3 at% Ti measured by microprobe analysis in a 45 mg droplet after an experiment lasting 300 min at 1250 °C (Fig. 2c) showing that a significant Ti depletion in the drop (from 4.5 at% to about 0.3 at% Ti) occurs when an interfacial layer of about 30 μm thick is formed at the interface (see Fig. 2a).

A final remark concerns the curvature of metal/reaction product interface which can be easily seen in Fig. 2a. This curvature is the result of mechanical stresses generated during cooling due to the very different thermal expansion coefficient of ceramic and metallic phases.

3.2.2. Effect of reaction time

Regardless of the reaction time at 1250 °C, the microstructure of the reaction layer is similar to that described previously (see Fig. 3a) and the layer thickness is almost uniform over most of the interface around the centre of the drop.

Table 1 summarises the mean values of e_{centre} and e_{max} obtained for reaction times up to 300 min. The maximum reaction layer thickness is always observed close to the triple line (Fig. 2a and b) for long-term experiments ($t \geq 35$ min), with a $e_{\text{max}}/e_{\text{centre}}$ ratio varying between 1.5 and 2. Conversely, for short-term experiments ($t \leq 10$ min), is not easy to detect such a maximum because of the relatively high scattering of e values (see Table 1).

The values of the reaction product thickness at the centre of the drop (e_{centre}) are plotted against time in Fig. 4 (black points). From this figure, it is difficult to describe the growth kinetics of the layer by a simple law (parabolic or linear), even if the Ti depletion in the drop during the reaction is taken into account. The black points in Fig. 4 show that the growth kinetics of the layer is rapid for reaction times lower than 50 min (growth rate $de/dt \approx 5 \text{ nm s}^{-1}$) and afterwards it slows down significantly.

3.2.3. Effect of temperature

Experiments with the same Ni–12Si–4.5Ti alloy on AlN were performed at three different temperatures for the same reaction

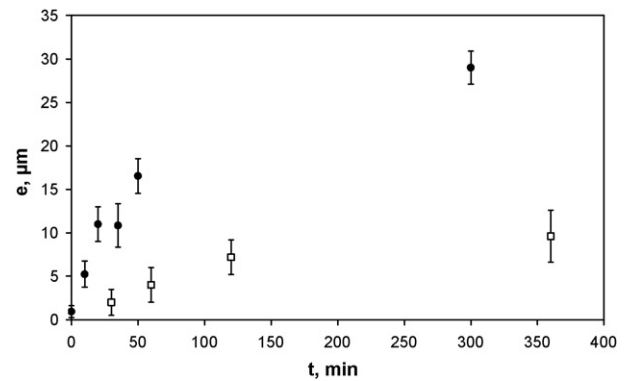


Fig. 4. Thickness of the reaction product at the centre of the drop (e) versus holding time at 1250 °C for experiments performed in a metallic furnace under a vacuum of 10^{-5} Pa (●) and in an alumina chamber furnace in a vacuum of 10^{-4} Pa (□). M–12Si–4.5Ti alloy on AlN.

time of 50 min. The effect of temperature on the thickness of the reaction layer at the centre of the drop was found to be weak, the layer thicknesses being $e_{\text{centre}} = 16.2 \pm 3.9 \mu\text{m}$, $16.5 \pm 2 \mu\text{m}$ and $19.9 \pm 4.1 \mu\text{m}$ at $T = 1215 \text{ °C}$, 1250 °C and 1300 °C , respectively. In view of the scattering of these reaction layer thickness values, it is difficult to quantify the temperature effect on the growth kinetics of the layer, however from these results it appears that the activation energy of the growth process is some tens of kJ mole^{-1} or less.

3.3. Alumina furnace ($P = 10^{-4}$ Pa)

3.3.1. Effect of time

Regardless of the reaction time, the microstructure of the reaction product is very similar to that observed for experiments performed in the metallic furnace (see Fig. 3a). Moreover, the reaction layer presents a similar profile to that observed previously (metallic furnace) with the $e_{\text{max}}/e_{\text{centre}}$ ratio varying between 1.5 and 3. Table 2 summarises the experimental results

Table 2
Thickness of the reaction layer formed at the M–12Si–4.5Ti/AlN interface at the centre of the drop (e_{centre}) and maximum of this thickness observed at a region close to the triple line (e_{max}) – see Fig. 2a and b – for different reaction times at 1250 °C

t (min)	30	60	120	360
e_{centre} (μm)	2 ± 1.5	4 ± 2	7.2 ± 2	9.6 ± 3
$e_{\text{max}}^{\text{a}}$ (μm)	Broken sample	7.2 ± 2	18.5 ± 2	29.5 ± 10.8

Experiments performed in an alumina chamber furnace ($P = 10^{-4}$ Pa).

^a Mean value calculated from two maxima formed to the left and right of the interface (see Fig. 2a).

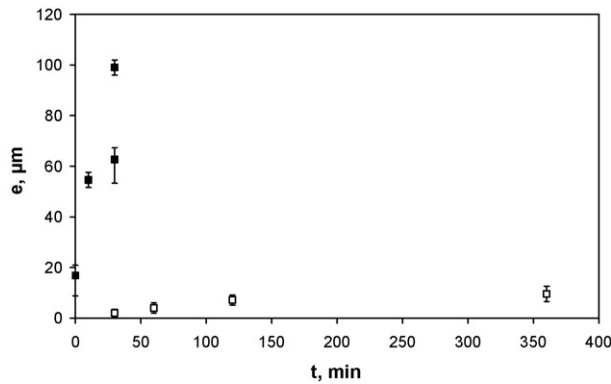


Fig. 5. Thickness of the reaction product at the centre of the drop (e) versus holding time at 1250 °C for experiments performed in an alumina chamber furnace. M–12Si–4.5Ti/AlN (□) and M–12Si–10Ti/AlN (■) samples.

(thickness of reaction layer at the drop centre and its maximum close to the triple line) for M–12Si–4.5Ti alloy on AlN at 1250 °C for reaction times varying from 30 min to 360 min.

Fig. 4 compares the variation with time of e_{centre} for experiments performed in both furnaces. This figure clearly shows that, for short-reaction times (<60 min), the growth kinetics of the reaction layer for experiments performed in the alumina furnace ($de/dt \approx 1 \text{ nm s}^{-1}$) is lower by half an order of magnitude than for experiments performed in the metallic furnace ($de/dt \approx 5 \text{ nm s}^{-1}$).

3.3.2. Effect of Ti content

Experiments performed at 1250 °C with M–12Si–10Ti alloy on AlN showed that an increase in the Ti content from 4.5 at% to 10 at% leads to a dramatic increase in the interfacial reactivity (reaction layer 60–100 μm thick after 30 min at 1250 °C compared to only 10 μm thick for M–Si–4.5Ti alloy after 360 min at the same temperature). Nevertheless, the morphology and microstructure of the reaction product are similar to those observed with M–12Si–4.5Ti alloy and described previously.

A plot of reaction layer thickness at the drop centre versus reaction time is shown in Fig. 5 for both alloys. This figure shows that the growth kinetics of the layer for M–12Si–10Ti alloy ($de/dt \approx 30 \text{ nm s}^{-1}$) is more than one order of magnitude higher than that of the M–12Si–4.5Ti alloy ($de/dt \approx 1 \text{ nm s}^{-1}$). Note that with M–12Ni–10Ti alloy the reactivity is so high that during heating, between the melting point of the alloy ($\approx 1170 \text{ °C}$) and the working temperature (1250 °C), the reaction layer grows up to 18 μm in less than 6 min. A Ti mass balance based on the formation of a 100 μm thick reaction layer for a 70 mg droplet shows that the quasi-totality of Ti (10 at%) initially contained in the alloy has reacted with the AlN substrate.

3.3.3. Experiments with Ag–Zr and Au–Ni–Ti alloys

Fig. 6 gives SEM micrographs of a cross-section of Au–Ni–5 at% Ti/AlN sample after 30 min at 1020 °C (Fig. 6a) and of Ag–1% Zr/AlN sample after a 10 min experiment at 970 °C (Fig. 6b). Both experiments were performed in an alumina furnace with alloy masses of about 50 mg.

For the Au–Ni–5 at% Ti alloy, the reaction product is 20–25 μm thick and it appears to consist of titanium nitride grains separated by metallic films a few hundreds of nm thick (cf. Fig. 6a). Moreover, the inert micrometric Y_2O_3 particles, initially included in AlN substrate, are observed all over the reaction layer.

In the case of Ag–1 at% Zr alloy, a continuous reaction layer, 0.2–0.5 μm thick, appears at the interface after 10 min at 970 °C (cf. Fig. 6b). (This short time was used to minimise evaporation of silver occurring in high vacuum.) The layer is too thin to allow a quantitative determination of its composition by X-ray micro-analysis. However, a line analysis by EDS clearly indicates the presence of Zr in the layer and the absence of Ag. In order to determine the phase formed at the interface, a second experiment was performed with the same alloy but with a larger mass (150 mg) leading to a larger interfacial area, thereby allowing a low-angle X-ray diffraction analysis to be carried out. This analysis performed on the interfacial layer after elimination by chemical dissolution of the Ag–Zr alloy clearly showed the formation of the ZrN compound. Note that for this system the reaction layer thickness is one to two orders of magnitude lower than for the Au–Ni–Ti/AlN system. This difference is not due to different reaction times (10 min against 30 min). Indeed, by assuming parabolic growth of the ZrN layer, the ZrN thickness after 30 min would be of the order of 1 μm which is still much thinner than the 20–25 μm observed with the Au–Ni–Ti alloy.

3.4. Summary of experimental results

The main experimental results of this study, in terms of reactivity at the centre of the drop and for short-time experiments ($t \leq 60 \text{ min}$), are summarised as follows:

- The reaction layer at the M–Si–Ti/AlN interface consists of titanium nitride grains separated by metallic films a few hundreds of nm thick. Inert micrometric Y_2O_3 particles, initially included in AlN substrate, are observed all over the layer.
- The reactivity between the M–12Si–4.5Ti alloy and AlN under high vacuum (metallic furnace, $P = 10^{-5} \text{ Pa}$) at 1250 °C is very high: the average growth rate of the TiN reaction layer is about 5 nm s^{-1} leading to a thickness of about 16 μm after only 50 min of reaction.
- When the vacuum pressure in the furnace increases from 10^{-5} Pa to 10^{-4} Pa the initial growth rate decreases by a factor 5.
- The effect of temperature on the reaction layer growth rate is very small corresponding to activation energy of some tens of kJ mole^{-1} or less.
- An increase in the Ti content in the alloy from 4.5 at% to 10 at% leads to an increase in the reaction product growth rate by more than one order of magnitude.
- The thickness of the reaction layer formed with the Au–Ni–5% Ti alloy is one to two orders of magnitude higher than with the Ag–1 at% Zr alloy at temperatures close to 1000 °C.

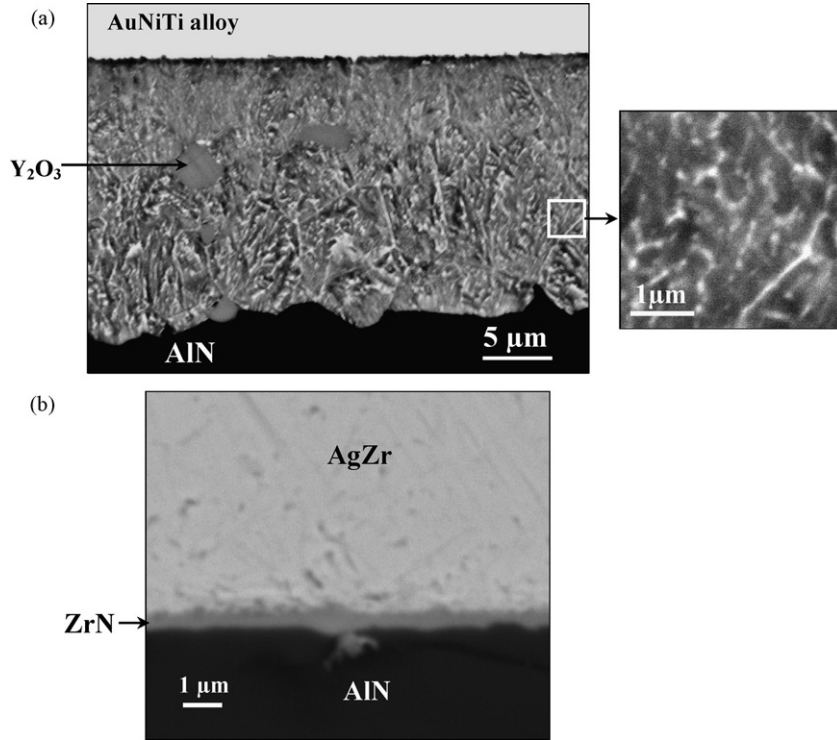


Fig. 6. SEM micrographs of a cross-section (a) of Au–Ni–5 at% Ti on AlN, 1020 °C, 30 min and (b) of Ag–1% Zr on AlN, 970 °C, 10 min (backscattered electron images). Experiments performed in an alumina furnace.

For all M–Si–Ti/AlN samples, the reaction layer thickness is almost uniform over most of the interface and presents a maximum in a region close to the triple line.

4. Discussion

4.1. Thermodynamics

Titanium contained in the alloy, reacts with AlN to form titanium nitride (which, for simplicity, is assumed to be stoichiometric):



At equilibrium, the mole fractions of Ti and Al in the alloy are related by:

$$\frac{x_{\text{Ti}}^{\text{eq}}}{x_{\text{Al}}^{\text{eq}}} = \frac{x_{\text{Ti}}^{\text{eq}}}{x_{\text{Ti}}^0 - x_{\text{Ti}}^{\text{eq}}} = \exp\left(\frac{\Delta_r G^\circ + \Delta \bar{G}_{\text{Al}}^{\text{xs}} - \Delta \bar{G}_{\text{Ti}}^{\text{xs}}}{RT}\right) \quad (2)$$

where x_{Ti}^0 is the initial Ti mole fraction in the alloy, $\Delta_r G^\circ$ is the standard Gibbs energy of reaction (1) and $\Delta \bar{G}_{\text{Al}}^{\text{xs}}$ and $\Delta \bar{G}_{\text{Ti}}^{\text{xs}}$ are the partial excess Gibbs energies of mixing of Ti and Al in the alloy, respectively.

The composition of the alloy at equilibrium will be evaluated semi-quantitatively by assuming that the alloy is diluted in Ti and Al. In this case the quantities $\Delta \bar{G}_{\text{Al}}^{\text{xs}}$ and $\Delta \bar{G}_{\text{Ti}}^{\text{xs}}$ can be approximated by their values at infinite dilution $\Delta \bar{G}_{\text{Al}}^{\text{xs},\infty}$ and $\Delta \bar{G}_{\text{Ti}}^{\text{xs},\infty}$. Moreover, the presence of Fe and Cr in the master alloy M is ignored, *i.e.*, the M–Si alloy will be replaced by the Ni–Si alloy. $\Delta \bar{G}_{\text{R}}^{\text{xs},\infty}$ (R = Ti or Al) is taken to be approximately equal to the

partial enthalpy at infinite dilution of R in the Ni–Si alloy $\Delta \bar{H}_{\text{R}}^\infty$ which, in turn, is evaluated from the partial enthalpies at infinite dilution of R in pure Ni and Si according to the equation¹⁷:

$$\Delta \bar{G}_{\text{R}}^{\text{xs},\infty} \approx \Delta \bar{H}_{\text{R}}^\infty = x_{\text{Ni}} \Delta \bar{H}_{(\text{R})_{\text{Ni}}}^\infty + x_{\text{Si}} \Delta \bar{H}_{(\text{R})_{\text{Si}}}^\infty - \Delta_{\text{m}} H_{(\text{Ni},\text{Si})} \quad (3)$$

$\Delta_{\text{m}} H_{(\text{Ni},\text{Si})}$ in Eq. (3) is the enthalpy of mixing of the Ni–Si alloy.

Combining Eqs. (2) and (3) and using the data of Table 3, the following relation between mole fractions of Ti and Al at equilibrium is obtained at $T = 1250$ °C:

$$\frac{x_{\text{Ti}}^{\text{eq}}}{x_{\text{Al}}^{\text{eq}}} = \frac{x_{\text{Ti}}^{\text{eq}}}{x_{\text{Ti}}^0 - x_{\text{Ti}}^{\text{eq}}} = 0.12 \quad (4)$$

The application of Eq. (4) with $x_{\text{Ti}}^0 = 0.045$ leads to $x_{\text{Ti}}^{\text{eq}} \approx 0.005$ (*i.e.*, 0.5 at% Ti). This result confirms the concentration of Ti in the drop bulk measured by microprobe analysis ($x_{\text{Ti}} \approx 0.3$ at% Ti) for M–12Si–4.5Ti/AlN sample maintained for 300 min at 1250 °C in the metallic furnace. Therefore, it can be concluded that thermodynamic equilibrium is nearly attained for the M–12Si–4.5Ti/AlN sample after 300 min at 1250 °C in the metallic furnace and for the M–12Si–10Ti/AlN sample after 30 min at 1250 °C in the alumina furnace. On the contrary, the M–12Si–4.5Ti/AlN system at 1250 °C in the alumina furnace is far from equilibrium even for long-term experiments (up to 360 min).

The same thermodynamic approach as described above is used for the Au–Ni–5 at% Ti/AlN and Ag–1 at% Zr/AlN systems. In the latter, zirconium contained in the alloy reacts with

Table 3

Summary of thermodynamic data used, the notations $\langle \rangle$, $()$ and $[]$ designate the solid, liquid and gaseous states, respectively

Reaction	ΔG° (in J)			Refs.
	970 °C	1020 °C	1250 °C	
$(\text{Al}) + 1/2[\text{N}_2] \rightarrow \langle \text{AlN} \rangle$	-183,360	-177,495	-150,548	[18]
$(\text{Ti}) + 1/2[\text{N}_2] \rightarrow \langle \text{TiN} \rangle$	-220,126	-215,385	-193,852	[18]
$\langle \text{Zr} \rangle + 1/2[\text{N}_2] \rightarrow \langle \text{ZrN} \rangle$	-249,716	-245,219	-224,274	[18]
$(\text{Ti}) \rightarrow (\text{Ti})$	3,518	3,336	2,472	[18]
$(\text{Zr}) \rightarrow (\text{Zr})$	6,899	6,615	5,164	[18]

Reaction	$\Delta \bar{G}_i^{\text{xs},\infty}$ (in J mol ⁻¹)	Refs.
$(\text{Ti}) \rightarrow (\text{Ti})_{\text{Ni}}$	$\Delta \bar{G}_{(\text{Ti})_{\text{Ni}}}^{\text{xs},\infty} = \Delta \bar{H}_{(\text{Ti})_{\text{Ni}}}^\infty = -130,000$	[19]
$(\text{Ti}) \rightarrow (\text{Ti})_{\text{Si}}$	$\Delta \bar{G}_{(\text{Ti})_{\text{Si}}}^{\text{xs},\infty} = \Delta \bar{H}_{(\text{Ti})_{\text{Si}}}^\infty = -146,000$	[20,21]
$(\text{Ti}) \rightarrow (\text{Ti})_{\text{Au}}$	$\Delta \bar{G}_{(\text{Ti})_{\text{Au}}}^{\text{xs},\infty} = \Delta \bar{H}_{(\text{Ti})_{\text{Au}}}^\infty = -98,500$	[22]
$(\text{Al}) \rightarrow (\text{Al})_{\text{Ni}}$	$\Delta \bar{G}_{(\text{Al})_{\text{Ni}}}^{\text{xs},\infty} = \Delta \bar{H}_{(\text{Al})_{\text{Ni}}}^\infty = -127,000$	[19]
$(\text{Al}) \rightarrow (\text{Al})_{\text{Si}}$	$\Delta \bar{G}_{(\text{Al})_{\text{Si}}}^{\text{xs},\infty} = \Delta \bar{H}_{(\text{Al})_{\text{Si}}}^\infty = -10,000$	[17]
$(\text{Al}) \rightarrow (\text{Al})_{\text{Au}}$	$\Delta \bar{G}_{(\text{Al})_{\text{Au}}}^{\text{xs},\infty} = \Delta \bar{H}_{(\text{Al})_{\text{Au}}}^\infty = -121,400$	[17]
$(\text{Zr}) \rightarrow (\text{Zr})_{\text{Ag}}$	$\Delta \bar{G}_{(\text{Zr})_{\text{Ag}}}^{\text{xs},\infty} = \Delta \bar{H}_{(\text{Zr})_{\text{Ag}}}^\infty = -13,000$	[23]
$(\text{Ni}) + (\text{Si}) \rightarrow (\text{Ni},\text{Si})$	$\Delta_m H = -132,000 x_{\text{Ni}} x_{\text{Si}}$	[24]
$(\text{Au}) + (\text{Ni}) \rightarrow (\text{Au},\text{Ni})$	$\Delta_m H = 8600 x_{\text{Au}} x_{\text{Ni}}$	[17]

AlN to form zirconium nitride:



The combination of Eqs. (2) and (3), with data from Table 3, leads to values of $x_{\text{Al}}^{\text{eq}}/x_{\text{Ti}}^0 = 0.993$ for Au–Ni–5 at% Ti/AlN at 1020 °C and $x_{\text{Al}}^{\text{eq}}/x_{\text{Zr}}^0 = 0.999$ for the Ag–1 at% Zr/AlN system at 970 °C meaning that reactions can proceed fully in both systems.

4.2. Kinetics

4.2.1. Reactional scheme

As described above in Section 3, regardless of the experimental conditions (atmosphere, temperature, time, Ti content), the microstructure of the reaction layer formed between M–12Si–Ti alloys and AlN is similar (see Fig. 3a): it consists of TiN grains separated by metallic films a few hundreds of nm thick. In addition, inert micrometric Y₂O₃ particles can be observed. In this system, Y₂O₃ particles can play the role of inert markers in order to determine the interface where reaction (1) takes place:

- (i) if reaction (1) takes place at the liquid/TiN interface, Y₂O₃ particles initially contained in the AlN substrate will accumulate at the AlN/TiN interface, otherwise;
- (ii) if reaction (1) takes place at the TiN/AlN interface between AlN and Ti arriving by diffusing through the reaction layer, these particles will stay dispersed throughout this layer. The experiment clearly indicates that Y₂O₃ particles are observed all over the reaction layer (see Fig. 3b) proving that reaction (1) takes place at the TiN/AlN interface.

The very high reactivity observed in this system is likely to come from the fast liquid-state diffusion of reactive species in the liquid channels, several hundred nm thick, separating TiN

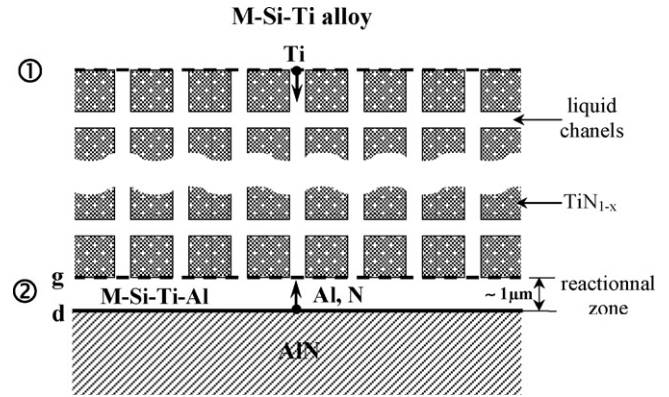


Fig. 7. Schematic representation of the M–Si–Ti alloy/AlN substrate system showing the reaction layer microstructure consisting of TiN grains separated by metallic films and the reactional zone (2) (see also Fig. 3a).

grains in the reaction zone (see Fig. 3a) and not by solid-state diffusion. The diffusion coefficients in the liquid alloys are in fact several orders of magnitude higher than the diffusion coefficients in the non-stoichiometric mono-crystalline titanium nitride (see Table 4).

The same conclusions can be drawn for the Au–Ni–5 at% Ti/AlN system for which the high value of the reaction layer thickness (20–25 μm) obtained after only 30 min at 1020 °C (see Fig. 6a) is close to the expected thickness at thermodynamic equilibrium (30–35 μm) indicating that reaction in this system is not far from equilibrium. Conversely, the observed thickness of the ZrN layer formed at the Ag–1 at% Zr/AlN interface (0.2–0.5 μm) is at least one order of magnitude lower than its value expected at thermodynamic equilibrium (about 5 μm). This considerable difference in reactivity between these two systems cannot be due to the difference in the driving force of transformation which is in fact much higher in the Ag–Zr/AlN system. Indeed, the thermodynamic activity of Ti in the Au–Ti–5 at% Ti alloy ($a_{\text{Ti}} = 1.5 \times 10^{-6}$) is three orders of magnitude lower than that of Zr in the Ag–1 at% Zr alloy ($a_{\text{Zr}} = 2.8 \times 10^{-3}$). Moreover, the standard Gibbs energy of reaction (1) $\Delta G_1^0 = -41226 \text{ J mol}^{-1}$ is in absolute value much lower than that of reaction (5) $\Delta G_5^0 = -73255 \text{ J mol}^{-1}$ (the above thermodynamic quantities are calculated by using data from Table 3). This marked difference between reactivities in these two systems is in reality due to differences in reaction product microstructure. Indeed, in the Au–Ni–Ti/AlN system, the grain boundaries of the reaction product (TiN) are perfectly wetted by the liquid alloy thus allowing fast liquid-state diffusion through the reaction layer, whereas in the Ag–Zr/AlN system, the ZrN reaction layer is impervious and constitutes a diffusion barrier, which makes sense given that the diffusion coefficient in ZrN is very low (see Table 4).

Based on these observations and statements, the M–Si–Ti alloy/AlN system can be schematically represented as shown in Fig. 7 (the same scheme also applies for the Au–Ni–Ti/AlN system). In view of Fig. 3a, showing that a large part of the AlN/layer interface is covered by metallic inclusions a few micrometers in size, and for the sake of simplicity, it has been assumed that, at this interface, AlN is totally covered by the liquid alloy. Accord-

ing to this scheme, the overall reaction of Ti with AlN leading to the formation of TiN, initially involves the dissolution of AlN in the liquid alloy at the dissolution interface (d), after which N migrates by short-range diffusion towards the growth interface (g) where it reacts with Ti arriving from the liquid bulk by long-range diffusion.

In the framework of this description, the growth rate of the reaction layer in a “clean system” (*i.e.*, without intervention of any impurity), may be limited by one of the two possible phenomena: (i) Liquid-state diffusion of species participating in the reaction (1), *i.e.*, of Ti from the drop bulk to the reaction interface (or of Al in the opposite sense), or (ii) Local reaction kinetics at the AlN/liquid interface, *i.e.*, AlN dissolution at the AlN/liquid interface or TiN growth at the liquid/TiN interface (see Fig. 7).

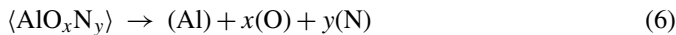
The activation energy for liquid-state diffusion in metallic alloys is low (up to some tens of kJ mole⁻¹). This fact is compatible with the weak effect of temperature on reaction kinetics found experimentally. However, as shown in Appendix A, the limitation by liquid-state diffusion of Ti (or Al) is highly unlikely. Moreover, none of the above two mechanisms is compatible with the following experimental facts:

- When the vacuum pressure decreases (from 10⁻⁴ Pa to 10⁻⁵ Pa) the reaction layer growth rate increases by a factor of 5 while the microstructure of the layer does not change.
- The existence of a maximum reaction layer thickness at a region close to the triple line despite the fact that the reaction time in this zone is lower than that in the centre of the drop.

4.2.2. Limitation by liquid-state diffusion of oxygen

Conversely, the experimental facts (a) and (b) are compatible with the assumption of kinetic control by liquid-state diffusion of oxygen from the AlN/reaction layer interface to the furnace atmosphere. We recall that AlN substrates contain about 1 wt% oxygen either in the AlN lattice or at grain boundaries (see Section 2). If the evacuation of oxygen from the reaction interface to the furnace atmosphere is slow, its accumulation at this interface can lead to the formation of Al oxynitrides which can act as barrier to AlN dissolution.¹³

Fig. 8 gives a schematic representation of the reactional zone where AlN is considered to be partially covered by Al oxynitride particles. The AlN dissolution rate in the liquid alloy then depends on the dissolution rate of these particles in the alloy according to the reaction (6):



The following section discusses successively in more detail the effect of the furnace atmosphere, Ti content in the alloy as well as geometrical configuration of the alloy/AlN system on the growth kinetics of the reaction layer where this growth is

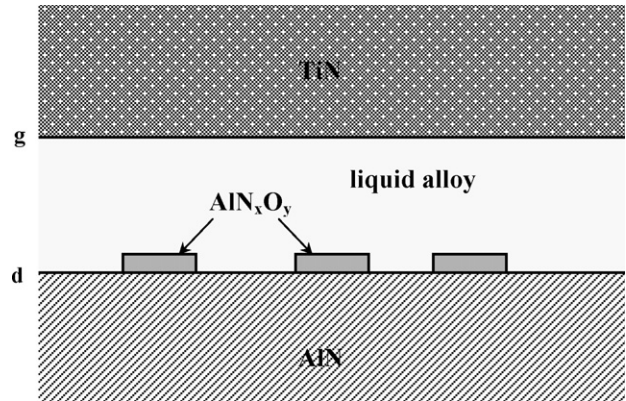


Fig. 8. Schematic representation of the reactional interface (noted (2) in Fig. 7) where AlN is considered to be partially covered by Al oxynitride particles.

controlled by liquid-state diffusion of oxygen contained as an impurity in AlN.

4.2.2.1. Effect of furnace atmosphere. The dissolution of AlN in the liquid alloy at the AlN/liquid alloy interface leads to a local increase in oxygen content at this interface. The oxygen then diffuses through the liquid channels of the reaction layer towards the drop and afterwards towards the liquid/vapour interface. When a quasi-steady state is attained, the variation in oxygen content in the liquid alloy from the AlN/reaction product interface (x_{O}^*) to the liquid/vapour surface (x_{O}^{LV}) can be represented schematically as shown in Fig. 9 (x_{O}^{LV} is affected by the furnace atmosphere while x_{O}^* is fixed by reaction (6)). This quasi-steady state is defined by the equality of diffusion flux (Φ_{diff}) and dissolution flux of oxygen (Φ_{diss}) at the AlN/reaction product interface:

$$\Phi_{\text{diss}} = \Phi_{\text{diff}} = D_{\text{O}} \cdot \frac{x_{\text{O}}^* - x_{\text{O}}^{\text{LV}}}{V_{\text{liq}}^{\text{m}} \cdot h} \quad (7)$$

where h is the drop height, D_{O} is the diffusion coefficient of oxygen in the liquid alloy and $V_{\text{liq}}^{\text{m}}$ is the liquid alloy molar volume.

When the vacuum pressure decreases, x_{O}^{LV} decreases too, consequently, according to Eq. (7) and for a given x_{O}^* , the oxygen dissolution flux (*i.e.*, the AlN dissolution flux) will increase, thus leading to an increase in the growth kinetics of the reaction layer.

4.2.2.2. Effect of Ti content. An increase in Ti content in the M–Si–Ti alloy leads to a huge decrease in the thermodynamic activity of oxygen (a_{O}) in this alloy. Indeed, the very strong interactions between titanium and oxygen atoms in molten nickel, expressed by a very negative value of their first-order interaction coefficient $\varepsilon_{\text{O}}^{\text{Ti}} = -86$,³¹ lead to a significant decrease in the

Table 4

Some values of diffusion coefficients in liquid alloys and in non-oxide ceramics at $T = 1200^\circ\text{C}$ except for SiC ($T = 1850^\circ\text{C}$)

	Liquid alloys	Cr ₃ C ₂	TiN	ZrN	TiC	SiC
D (m ² s ⁻¹)	10 ⁻⁹ to 10 ⁻⁸	3.4 × 10 ⁻¹⁵	7 × 10 ⁻¹⁹	1.2 × 10 ⁻¹⁶	10 ⁻¹⁶	2.3 × 10 ⁻¹⁸
Refs.	[25]	[26]	[27]	[28]	[29]	[30]

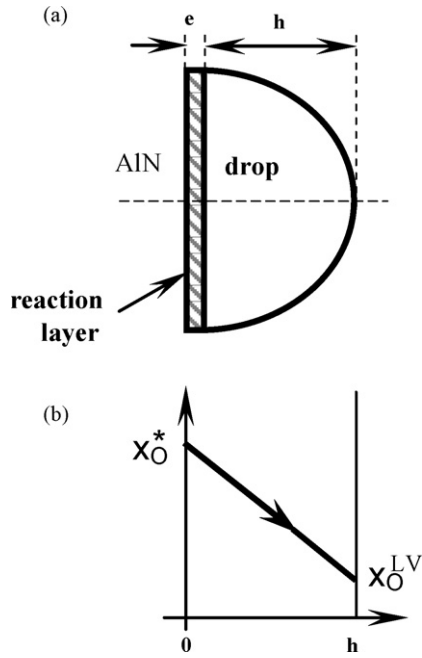


Fig. 9. (a) Schematic representation of the drop/AlN substrate system. (b) Schematic representation of oxygen concentration profiles across the system at the centre of the drop for $e \ll h$. e is the thickness of the reaction layer and h the drop height. x_O^* and x_O^{LV} are the oxygen content in the alloy at the AlN/layer interface and liquid/vapour interface, respectively.

activity coefficient of oxygen (γ_O) with Ti mole fraction:

$$\ln \gamma_O = \ln \gamma_O^\infty + \varepsilon_O^{\text{Ti}} x_{\text{Ti}} = \ln \gamma_O^\infty - 86x_{\text{Ti}} \quad (8)$$

where γ_O^∞ is the infinite dilution activity coefficient of oxygen in liquid Ni.

It is assumed that thermodynamic equilibrium is reached for reaction (6) at the AlN_xO_y /liquid alloy interface (see Fig. 7), *i.e.*, for a fixed temperature the oxygen activity ($a_O^* = \gamma_O^* x_O^*$) is fixed at this interface. Moreover, for the sake of simplicity, a diluted solution behaviour for Ni–Ti alloys is also assumed, *i.e.*, Eq. (8) is considered to be valid (at least semi-quantitatively) for a Ti content as high as 10 at%. Then, according to Eq. (8), if Ti content in the alloy increases from 4.5 at% to 10 at%, the oxygen coefficient activity (γ_O) decreases by a factor of about 100 meaning that, for a given T (*i.e.*, for a fixed a_O^*), the oxygen content at the AlN_xO_y /liquid alloy interface (x_O^*) will increase by the same factor. Consequently, according to Eq. (7) the oxygen dissolution flux will increase, thus leading to an increase in the growth kinetics of the reaction layer.

4.2.2.3. Effect of geometrical configuration of the alloy/substrate system. If oxygen diffusion through the drop (from the reaction interface to the liquid/vapour surface) is a limiting factor, then the thickness of the reaction product in a wetting experiment would vary between the centre of the drop and the triple line. This is because the thickness of the reaction product at any point of the interface in a sessile drop experiment is the result of two effects acting in the opposite sense:

- (i) The first is the effect of the reaction time. This reaction time is maximum at the drop centre and zero at the triple line and as a consequence the layer thickness is maximum at the drop centre and zero at the triple line.
- (ii) The second effect results from the oxygen diffusion distances in the drop. These distances are maximum at the centre of the drop and zero at the triple line.

During real wetting experiments these two effects occur simultaneously thus providing a possible explanation for the maximum thickness of the interfacial layer between the centre of the drop and the triple line observed experimentally.

5. Concluding remarks

The results obtained in this study have revealed the predominant role in interfacial reactivity of oxygen and wetting of reaction product grain boundaries by the liquid alloy. Oxygen is a common impurity of furnace atmospheres and it is well established that it can have a considerable effect on the surface properties of metals and non-oxide ceramics even at partial pressures as low as 10^{-10} bar.¹ Moreover, oxygen is contained in most predominantly covalent ceramics, especially when these materials are processed by sintering. Until now it has been established that even nanometric oxide layers formed on the surface of these ceramics can act as barriers to wetting, especially at low ($\approx 600^\circ\text{C}$) and moderate ($\approx 1200^\circ\text{C}$) temperatures.^{1,32} The present work demonstrates that this factor can also affect and even control reactivity at metal/ceramic interfaces.

The perfect wetting of reaction product grain boundaries by the liquid alloy provides fast diffusion paths for reacting species and can, as a consequence, exacerbate reactivity. For example, diffusion coefficients D in molten alloys at $T \approx 1200^\circ\text{C}$ are 6–10 orders of magnitude greater than typical values of D in ceramics such as TiC, ZrN or SiC (see Table 4). As a consequence, in the absence of perfect wetting of grain boundaries, once a continuous layer of such a compound has formed at the interface, the growth rate is substantially reduced and may even drop to zero. This type of layer therefore acts in a similar way as passive oxide films formed on stainless steels or silicon carbide surfaces which protect the underlying materials from further oxidation.

Transitions from partial wetting to perfect wetting of grain boundaries by liquid metals have been observed for several liquid metal/solid metal couples, occurring as a function of temperature or system composition.^{33–35} However, to the author's knowledge, no similar studies exist for liquid metal/ceramic systems. One can only anticipate that, for a given ceramic, *i.e.*, for a given grain boundary energy σ_{GB} , good wetting of its surface by the liquid metal or alloy ($\theta \ll 90^\circ$) indicates a low metal/ceramic interfacial energy $\sigma_{\text{Me/Cer}}$ thus making it more likely that the condition of perfect wetting of grain boundaries $\sigma_{\text{GB}} > 2\sigma_{\text{Me/Cer}}$ will be satisfied. Low acute contact angles are often observed when the reaction product presents metallic features as in the case of Ti, Zr and Cr carbides, nitrides and borides.^{1,36} The $\text{Cu}_3\text{Ti}_3\text{O}$ compound also exhibits a metallic character and its formation at CuAgTi/alumina interfaces is responsible for the very low con-

tact angles obtained in this system.² Moreover, at a relatively low temperature (900 °C), thick layers of this compound were observed in the above system, while its microstructure clearly shows perfect wetting of its grain boundaries by the CuAgTi alloy.

Appendix A

If it is assumed that liquid-state diffusion of Ti (or Al) is the rate-limiting step of reaction (1), then thermodynamic equilibrium of this reaction is reached at the AlN/layer interface (see Fig. A.1) and, as long as x_{Ti} remains close to the initial Ti content x_{Ti}^0 , the variation in reaction layer thickness e with time t will obey a parabolic law:

$$e^2 \approx \alpha \cdot (x_{Ti}^0 - x_{Ti}^{eq}) \cdot D_{Ti} \cdot t \approx \alpha \cdot x_{Ti}^0 \cdot D_{Ti} \cdot t \quad (\text{A.1})$$

where $\alpha = 2(S_c/S_{tot})(V_{TiN}^m/V_{liq}^m)$. S_{tot} is the total area of the TiN/layer interface and S_c the liquid channel area in a section parallel to the interface. V_{TiN}^m and V_{liq}^m are the molar volumes of TiN and liquid, respectively. D_{Ti} is the diffusion coefficient of Ti in the liquid alloy.

The application of Eq. (A.1) for short-term experiments ($t < 60$ min, $x_{Ti} > 0.023$), with $V_{TiN}^m = 11.7 \text{ cm}^3 \text{ mol}^{-1}$, $V_{liq}^m = 7.4 \text{ cm}^3 \text{ mol}^{-1}$,³⁷ $S_c/S_{tot} > 0.05$ and $D_{Ti} \approx 5 \times 10^{-9} \text{ m}^2 \text{ s}^{-1}$ leads to a calculated value of e^2/t ratio: $(e^2/t)_{\text{calc}} > 20 \mu\text{m}^2 \text{ s}^{-1}$. This value is several orders of magnitude higher than the experimental values $(e^2/t)_{\text{exp}} \approx 6 \times 10^{-3} \mu\text{m}^2 \text{ s}^{-1}$ and $9 \times 10^{-2} \mu\text{m}^2 \text{ s}^{-1}$ obtained for M–12Si–4.5Ti/AlN samples in metallic and alumina furnaces, respectively.

This clearly shows that reaction product growth kinetics is not controlled by liquid-state diffusion of Ti (the same conclusion holds for diffusion of Al). As a consequence, the Ti and Al contents in the alloy at the AlN/reaction layer interface, x_{Ti}^* and x_{Al}^* , are almost equal to the Ti and Al contents in the drop bulk, respectively.

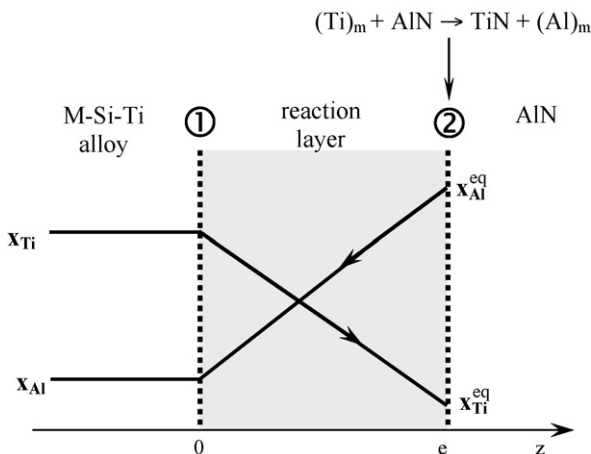


Fig. A.1. Schematic representation of Ti and Al content profiles across the reaction layer in the M–Si–Ti/AlN system when the rate-limiting step of the reaction (1) is assumed to be the liquid-state diffusion of elements participating in reaction (1) (Ti or Al). x_i and x_i^{eq} are the concentrations of i ($i = \text{Ti, Al}$) in the drop bulk and at the AlN/layer interface, respectively.

References

- Eustathopoulos, N., Nicholas, M. and Drevet, B., *Wettability at High Temperature*. Pergamon Materials Series, vol. 3. Oxford, UK; 1999, pp. 198–261.
- Voytych, R., Robaut, F. and Eustathopoulos, N., *Acta Mater.*, 2006, **54**, 2205–2214.
- Eustathopoulos, N., *Curr. Opin. Solid State Mater. Sci.*, 2005, **9**, 152–160.
- Howe, J. M., *Int. Mater. Rev.*, 1993, **38**, 233–256.
- Xiao, P. and Derby, B., *Acta Mater.*, 1998, **46**, 3491–3499.
- Xiong, H. P., Chen, B., Kang, Y. S., Mao, M., Kawasaki, A., Okamura, H. and Watanabe, R., *Scripta Mater.*, 2007, **56**, 173–176.
- Zhuravlev, V., Prokopenko, A. and Koval, A., *Trans. JWRI*, 2001, **30**, 131–135.
- Liang, Y. N., Osendi, M. I. and Miranzo, P. J., *Eur. Ceram. Soc.*, 2003, **23**, 547–553.
- Nicholas, M. G., Mortimer, D. A., Jones, L. M. and Crispin, R. M. J., *Mater. Sci.*, 1990, **25**, 2679–2689.
- Tomsia, A. P. and Loehman, R. E., *Ceram. Eng. Sci. Proc.*, 1989, **10**, 1631–1654.
- Benko, E., *Ceram. Int.*, 1995, **21**, 303–307.
- Schmid-Fetzer, R. and Bhanumurthy, K., *Comp.: Part A*, 2001, **32**, 569–574.
- Koltsov, A., Dumont, M., Hodaj, F. and Eustathopoulos, N., *Mater. Sci. Eng. A*, 2006, **A415**, 171–176.
- Baffie, T., Contribution à l'amélioration des propriétés thermiques d'assemblages cuivre/nitride d'aluminium polycristallin destinés à l'électronique de puissance. PhD Thesis. Institut National Polytechnique de Grenoble, France; 2000, p. 97.
- Rozzaza Prin, G., Baffie, T., Jeymond, M. M. and Eustathopoulos, N., *Mater. Sci. Eng. A*, 2001, **A298**, 34–43.
- Xiao, P. and Derby, B., *Acta Mater.*, 1996, **44**, 307–314.
- Kubashevski, O., Alcock, C. B. and Spencer, P. J., *Materials Thermochemistry (6th edition)*. Pergamon Press, 1993, pp. 60–61.
- Nist-Janaf Thermochemical Tables, J. Phys. Chem. Ref. Data, Monograph No. 9 (fourth edition). American Chemical Society, American Institute of Physics, New York; 1998.
- Dupin, N., Contribution à l'évaluation thermodynamique des alliages polycristallins à base de nickel. PhD Thesis. Institut National Polytechnique de Grenoble, France; 1995, p. 225, 240.
- Sudavtsova, V. S., Batalin, G. I. and Tutevich, V. S., *Inorg. Mater.*, 1985, **21**, pp. 670–676.
- Esin, Y. O., Valishev, M. G., Ermakov, A. F., Gel'd, P. V. and Petrushevskiy, M. S., *Russ. Metall.*, 1981, **2**, 71–72.
- Kleppa, O. J. and Topor, L., *Metall. Trans. A*, 1985, **16A**, 93–99.
- Fitzner, K. and Kleppa, O. J., *Metall. Trans. A*, 1992, **23A**, 997–1003.
- an Mey, S., *Z. Metallkunde*, 1986, **77**(12), 805–810.
- Geiger, G. H. and Poirier, D. R., *Transport Phenomena in Metallurgy*. Addison-Wesley Publishing Company, Reading, MA, 1980, pp. 455–463.
- Mayr, W., Lengauer, P., Ettmayer, P., Rafaja, D., Bauer, J. and Bohn, M. J., *Phase Equilib.*, 1999, **20**(1), 35–44.
- Abautret, F. and Eveno, P., *Revue de Physique Appliquée*, 1990, **25**(11), 1113–1120.
- Matzke, H., *Adv. Ceram.*, 1987, **23**, 617–645.
- van Loo, F. J. J. and Bastin, G. F., *Metall. Trans. A*, 1989, **20A**, 403–411.
- Matzke, H., *Defect Diff. Forum*, 1992, **83**, 111–130.
- Dashevskii, V. Y., Makarova, N. N., Grigorovich, K. V. and Kashin, V. I., *Rasplavy (in Russian)*, 1999, **4**, 52–61.
- Rado, C. and Eustathopoulos, N., *Interface Sci.*, 2004, **12**, 85–92.
- Eustathopoulos, N., *Int. Met. Rev.*, 1983, **28**, 189–210.
- Rabkin, E., Shvindlerman, L. and Straumal, B., *Int. J. Modern Phys. B*, 1991, **5**, 2989–3028.
- Straumal, B., Gust, W. and Molodov, D., *J. Phase Equilib.*, 1994, **15**, 386–391.
- Naidich, Y., *In Progress in Surface and Membrane Science*, ed. D. A. Cadenhead and J. F. Danielli. Academic Press, New York, 1981, pp. 439–447.
- Brandes, E. A. and Brook, G. B., ed., *Smithells Metals Reference Book*. seventh edition Butterworth-Heinemann, 1998, pp. 14–6, 27–4.